Calcium- and Membrane-Induced Changes in the Structure and Dynamics of Three Helical Hairpins in Annexin B12[†]

Jose Mario Isas,[‡] Yujin E. Kim,[‡] Christine C. Jao,[‡] Prabhavati B. Hegde,[‡] Harry T. Haigler,*[,§] and Ralf Langen*[,‡]

Department of Biochemistry and Molecular Biology, Keck School of Medicine of the University of Southern California, Los Angeles, California 90033, and Department of Physiology and Biophysics, University of California, Irvine, California 92697

Received August 30, 2005; Revised Manuscript Received October 19, 2005

ABSTRACT: Annexins are a family of soluble proteins that can undergo reversible Ca^{2+}-dependent interaction with the interfacial region of phospholipid membranes. The helical hairpins on the convex face of the crystal structure of soluble annexins are proposed to mediate binding to membranes, but the mechanism is not defined. For this study, we used a site-directed spin labeling (SDSL) experimental approach to investigate Ca^{2+} and membrane-induced structural and dynamic changes that occurred in the helical hairpins encompassing three of the four D and E helices of annexin B12. Electron paramagnetic resonance (EPR) parameters were analyzed for the soluble and Ca^{2+}-dependent membrane-bound states of the following nitroxide scans of annexin B12: a continuous 24-residue scan of the D and E helices in the third repeat (residues 219−242) and short scans encompassing the D−E loop regions of the first repeat (residues 68−74) and the fourth repeat (300−305). EPR mobility and accessibility parameters of most sites were similar when the protein was in solution or in the membrane-bound state, and both sets of data were consistent with the crystal structure of the protein. However, membrane-induced changes in mobility and accessibility were observed in all three loop regions, with the most dramatic changes noted at sites corresponding to the highly conserved serine and glycine residues in the loops. EPR accessibility parameters clearly established that nitroxide side chains placed at these sites made direct contact with the bilayer. EPR mobility parameters showed that these sites were very mobile in solution, but immobilized on the EPR time scale in the membrane-bound state. Since the headgroup regions of bilayer phospholipids are relatively mobile in the absence of annexins, Ca^{2+}-dependent binding of annexin B12 appears to form a complex in which the mobility of the D−E loop region of the protein and the headgroup region of the phospholipid are highly constrained. Possible biological consequences of annexin-induced restriction of membrane mobility are discussed.

The reversible binding of soluble cytosolic proteins to the interfacial region of specific subcellular membranes plays an important role in cell signaling and membrane trafficking. Membrane binding of peripheral proteins is often mediated by modular domains (*1*), but a few proteins, such as annexins, contain specific membrane binding activity within their core structures (*2*). High-resolution structural information about these proteins in the membrane-bound state is needed to understand the molecular mechanisms by which peripheral proteins interact with membranes, but obtaining these data has been technically challenging.

Annexins are a family of proteins that provide a regulated link between intracellular Ca^{2+} signaling and a number of membrane-related functions, including membrane domain organization, vesicular trafficking, and membrane fusion (*2*, *3*). The functional hallmark of annexins is reversible Ca^{2+}-dependent binding to the surface of membranes that contain negatively charged phospholipids (*4*). The Ca^{2+}-binding sites are located in the core domains of these proteins, which are composed of four repeats (or eight repeats in annexin A6) of a conserved ∼70-amino acid sequence. The existence of this tetrad of internal repeats in a broad phylogenetic range of organisms, including protists, plants, and animals, implies that this core structure serves to provide a highly conserved and fundamental physiological function (*5*).

High-resolution crystal structures of the soluble forms of many different annexin gene products show that all have nearly identical backbone folds (*4*). Furthermore, within any given annexin molecule, the four repeats have nearly identical structures (see the structure of annexin B12 in panels A and B of Figure 1). Each repeat consists of five α-helices, labeled A−E. X-ray studies of crystals prepared in the presence of high concentrations of Ca^{2+} identified three types of Ca^{2+}-binding sites in the short connecting loops between the A and B helices and between the D and E helices on the convex face of the protein (*4*). The interaction of annexins with membranes is proposed to be mediated via joint coordination of Ca^{2+} by the protein and by phosphoryl oxygen of the phospholipid headgroup in the bilayer (*6*). The site that is

[†] This work was supported by National Institutes of Health Grants GM 63915 (R.L.) and GM 55651 (H.T.H.).

* To whom correspondence should be addressed. R.L.: telephone: (323) 442-1323; fax: (323) 442-4404; e-mail: langen@usc.edu. H.T.H.: telephone: (949) 824-6304; fax: (949) 824-8540; e-mail: hhaigler@uci.edu.

[‡] Keck School of Medicine of the University of Southern California.

[§] University of California.

10.1021/bi051751m CCC: $30.25
Published on Web 11/24/2005

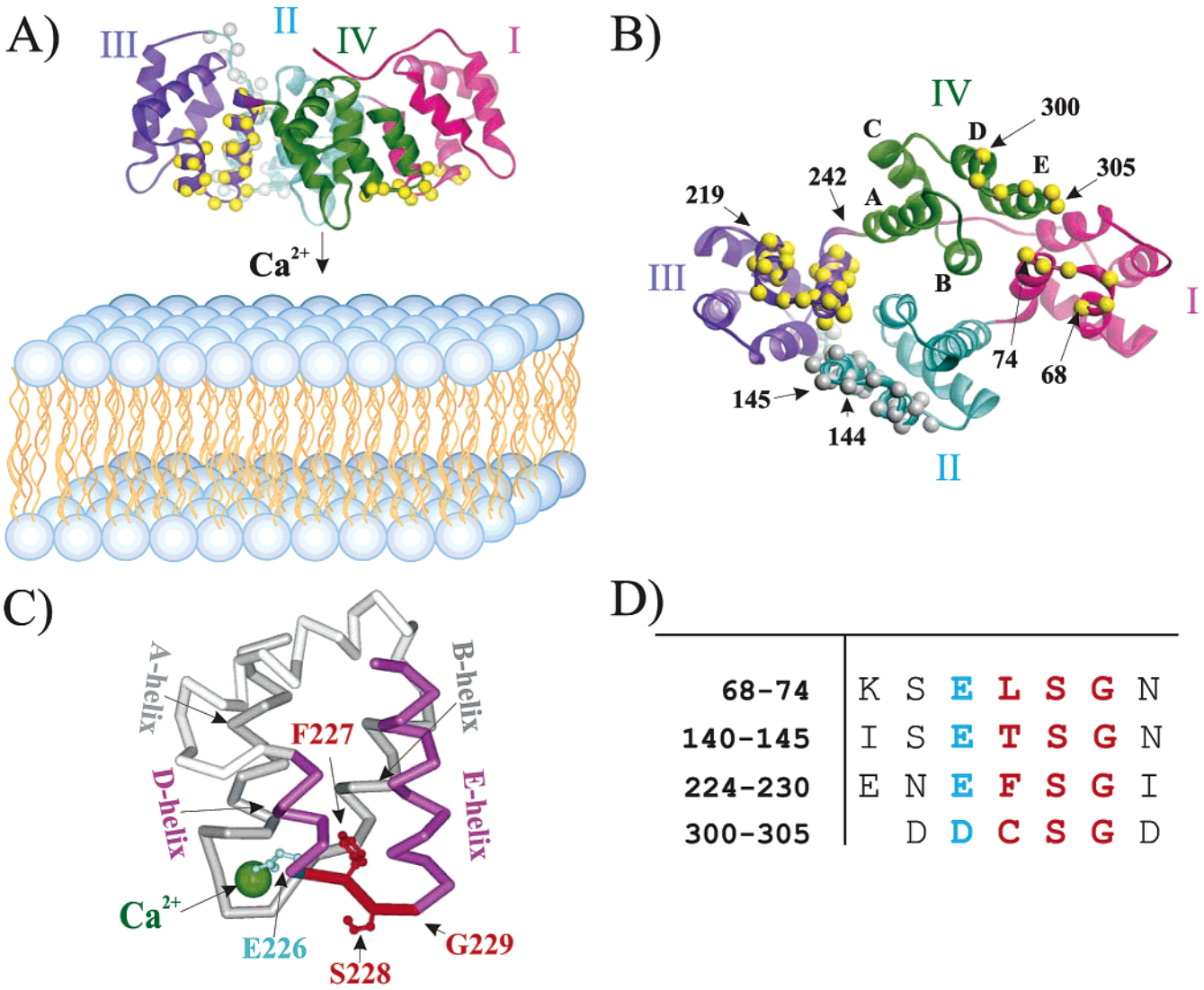

FIGURE 1: Structure of annexin B12. (A) Crystal structure of the annexin B12 monomer (ref *25* and PDB entry 1AEI) with the convex face that contains the Ca^{2+}-binding loops facing the bilayer. The four repeats of the core domain are labeled with Roman numerals and are shown in different colors. Yellow or gray spheres on α-carbons highlight areas analyzed by nitroxide scans in this study or in previous reports (*11*, *13*), respectively. (B) Model of annexin B12 as in panel A, but rotated 90° so that the Ca^{2+}-binding loops face the reader. (C) Crystal structure of the region of the third repeat of annexin B12 with residues 219−242 colored purple. Loop residues F227, S228, and G229 are highlighted. The green sphere is Ca^{2+} bound to a type II site formed, in part, by the side chain of E226 (light blue). (D) Amino acid sequence in and around the loops that connect the D and E helices in the four repeats of annexin B12. Residues colored blue contribute carboxylate side chains to type II Ca^{2+} sites. Residues in the D−E loops are colored red.

thought to be the most important in membrane binding has been named the "type II" site (*7*). Ca^{2+} at the type II site is coordinated by main chain carbonyl oxygen atoms in the A−B loop and a carboxylate group from a Glu or Asp side chain located at the end of the D helix (Figure 1D). The Glu/Asp is followed by a short loop composed of the highly conserved sequence -X-Ser-Gly (Ser is infrequently replaced with Thr). Numerous crystallography and mutagenesis studies suggest that the D−E loop regions play a critical role in Ca^{2+}-dependent interaction of annexins with membranes (see ref *8* for a review). Direct structural studies of membrane-bound annexins are now needed to evaluate these hypotheses and to further define the mechanism of protein−membrane interaction.

Using the interaction of annexin B12 with phospholipid vesicles as a model system, we have undertaken an extensive study designed to provide high-resolution structural and dynamic information that is needed to define the biophysical mechanisms by which annexins interact with membranes (*9*−*14*). The primary experimental approach in these studies was site-directed spin labeling (SDSL),[1] a method that is particularly useful for studying membrane proteins (*15*). This method involves the introduction of the paramagnetic nitroxide chain, R1 (see Figure 2), into proteins through the selective modification of unique cysteine residues that were

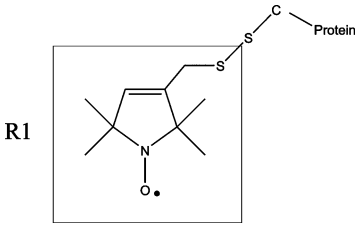

FIGURE 2: Structure of the R1 side chain.

[1] Abbreviations: PS, phosphatidylserine; PC, phosphatidylcholine; EPR, electron paramagnetic resonance spectroscopy; SDSL, site-directed spin labeling.

substituted into the protein by site-directed mutagenesis. The shape of the electron paramagnetic resonance (EPR) spectrum of the nitroxide-labeled protein reflects the mobility of the R1 side chain and can be used to evaluate local and backbone dynamics of the protein (*16*). The topography of membrane-associated proteins can be determined by EPR accessibility parameters (*17*). Nitroxide-scanning experiments, in which single native side chains are sequentially replaced with R1, can be used to evaluate secondary structure by analyzing periodic changes in EPR parameters as a function of sequence number (*11*).

Previous SDSL studies of annexin B12 showed that it exists in three structural forms: a soluble monomer (*9*, *11*), a Ca^{2+}-dependent peripheral membrane-bound trimer (*9*), and a transmembrane form that inserts into membranes at mildly acidic pHs in a Ca^{2+}-independent manner (*10*). The transmembrane form requires major inside-out refolding of annexin B12 (*12*) and is structurally very different from that in solution. In contrast, the Ca^{2+}-dependent membrane-bound form results in a structure with strong similarities to that of the X-ray structure of lipid-free protein (*13*).

A continuous nitroxide scan encompassing the D−E helical hairpin in the second repeat of annexin B12 was recently analyzed in solution and in the Ca^{2+}-dependent membrane-bound form (*11*, *13*). In both forms, the protein had a very similar backbone fold, but the dynamics of residues within the interhelical loop region were found to be strikingly different. While those residues were highly dynamic in solution, as generally observed for loop sites, membrane interaction induced a very strong immobilization. The degree of this immobilization has been unprecedented in SDSL studies of membrane-interacting sites, and it has been suggested (*13*) that these highly unusual properties could be related to the well-known ability of some annexins to strongly coordinate the lipid headgroups (*18*−*20*). On the basis of these results and the fact that all four D−E hairpins have highly similar structures (Figure 1A,B) and loop sequences (Figure 1D), it is possible that D−E loop regions from other repeats might have similar structural and dynamic features upon Ca^{2+}-dependent membrane interaction. In this case, the loop regions in the different repeats could act cooperatively in coordinating multiple Ca^{2+} ions and lipids. However, the Ca^{2+}-binding sites in annexin crystal structures are located on the convex face of the protein, and the bound Ca^{2+} cations that are thought to link the protein to membranes are not coplanar (*21*). The degree to which the protein curvature is retained in the Ca^{2+}-dependent membrane-bound form has not yet been clearly defined, and it has not yet been shown how this potential curvature mismatch affects the membrane interaction properties of the various loop regions. In particular, it is not yet known whether all repeats in annexins make direct contact with the bilayer following Ca^{2+}-dependent binding. To address this and other questions, this study focused on structural and dynamic changes induced in three D−E hairpins in annexin B12 by Ca^{2+}-dependent membrane binding. Combined with our previous study (*13*), these studies provide a comprehensive picture of the interaction of all four D−E helical hairpin regions with membranes.

A continuous 24-residue scan of the D and E helices in the third repeat (residues 219−242) and short scans encompassing the D−E loop regions of the first repeat (residues 68−74) and the fourth repeat (residues 300−305) were analyzed in solution at neutral pH after Ca^{2+}-dependent binding to membranes. The location of these regions in the crystal structure of annexin B12 is illustrated in panels A and B of Figure 1. The annexin B12 trimer is not shown because none of the regions scanned in this study are near the monomer−monomer interfaces in the trimer. Figure 1C presents a detailed view of the region of residues 219−242 of the protein, with the side chains of the type II Ca^{2+} site and loop residues highlighted. The amino acid sequence of all four D−E loops and adjacent regions of annexin B12 are shown in Figure 1D. Note that the Glu/Asp-X-Ser-Gly sequence is present in all D−E loops of annexin B12 (Figure 1D).

EPR studies of these three nitroxide scans of annexin B12 did not detect any significant structural changes in the backbone fold when the soluble protein underwent Ca^{2+}-dependent binding to membranes. EPR accessibility parameters unambiguously showed that all of the D−E loops made direct contact with membranes, and mobility parameters showed that all of the D−E loops were very dynamic in solution but immobilized on the EPR time scale following membrane binding. We conclude that Ca^{2+}-dependent interaction of annexin B12 with membrane phospholipids forms an immobile complex whose biological function may be to serve as a molecular fence that creates or maintains domains of a nonhomogeneous distribution of lipids and/or proteins in cellular membranes.

EXPERIMENTAL PROCEDURES

Annexin Expression and Purification. Site-directed mutagenesis by the Clontech (Palo Alto, CA) method was used to construct a series of 39 single-cysteine substitution mutants that correspond to residues 68−74, 218−244, and 300−304 of annexin B12 (*9*, *10*). Two native cysteines, 113 and 302, were replaced with Ala, resulting in the Cys-less mutant (C113A/C302A) that was the starting point for the above cysteine mutations (*9*, *10*). All mutations were confirmed by DNA sequencing. The annexin B12 mutants were expressed in recombinant bacteria and purified by reversible Ca^{2+}-dependent binding to phospholipid vesicles, followed by column chromatography, as previously described (*9*, *10*). The ANX12 concentration was determined by absorbance at 280 nm (extinction coefficient of 12 288 M^{-1} cm^{-1}).

Spin Labeling and EPR Measurements. The introduced cysteines were modified with spin-label (1-oxy-2,2,5,5-tetramethylpyrrolinyl-3-methyl)methanethiosulfonate, as previously described (*9*). Spin-labeled mutants of annexin B12 are designated by giving the sequence position of the cysteine substitution followed by the code of the nitroxide spin-label, R1. Spin-labeled proteins were stored frozen in diluted buffer at pH 7.4. Prior to use in EPR experiments, the spin-labeled proteins were concentrated in a Microcon YM-10 apparatus (Amicon) using a tabletop microfuge. Large vesicles with a lipid composition of phosphatidylserine (brain, catalog no. 840037, Avanti Polar Lipids, Alabaster, AL) and phosphatidylcholine (egg yolk, catalog no. 850355, Avanti Polar Lipids) at a 2:1 molar ratio were prepared according to the Reeves−Dowben protocol (*22*).

EPR experiments were performed on R1-labeled annexin B12 mutants (30 μg of protein) in buffer [20 mM Hepes and 100 mM NaCl (pH 7.4)] with phospholipid vesicles. The

molar ratio of protein to lipid was 1:500, and the binding of annexin 12 to the vesicles was induced with Ca^{2+} (1 mM). X-Band EPR spectra were obtained at room temperature using an EMX Bruker spectrometer. All spectra were obtained at an incident microwave power of 2 mW. For accessibility measurements, the oxygen concentration was that of oxygen in equilibrium with room air and the chelated nickel (NiEDDA) concentration was 3 mM. The scan width for EPR spectra was 100 G.

The fractional solvent accessibility for the native residues was computed from the crystal structure of a monomer of the crystallographic hexamer (PDB entry 1AEI) with MOLMOL (*23*) and a probe radius of 1.4 Å.

RESULTS

Preparation of Spin-Labeled Annexin B12. To investigate the structural and dynamic changes upon Ca^{2+}-dependent membrane interaction of annexin B12, we performed three separate nitroxide-scanning experiments. The most extensive nitroxide scan was performed by engineering single-Cys mutants into sites 219−242 of annexin B12, a region that encompasses the D−E helical hairpin of the third repeat (see Figure 1). In two additional nitroxide scans, single-Cys mutants were introduced into sites 68−74 and 300−305, regions that include the loops connecting the D and E helices in the first and fourth repeats of annexin B12, respectively (see Figure 1). Each of the Cys mutants was subsequently spin labeled to generate R1 (see Figure 2), and the EPR data were compared for soluble and membrane-bound annexin B12. R1 labeling did not appear to structurally or functionally alter 36 of these 37 sites, as evidenced by the fact that the R1-labeled derivatives, like wild-type annexin B12, underwent reversible Ca^{2+}-dependent binding to phospholipid under the conditions that were used (data not shown). However, R1-labeled position 71 was unstable and was excluded from further analysis.

R1 Mobility in the Nitroxide Scan of Residues 219−242 of Soluble Annexin B12. Figure 3A shows the EPR spectra for the R1 scan of residues 219−242. The black traces represent EPR spectra from soluble annexin B12 derivatives at pH 7.4, recorded in the presence of 30% sucrose, a commonly used reagent to inhibit protein tumbling. Under these conditions, the line shapes of the spectra predominantly reflect the mobility of the R1 side chain with respect to the protein and are no longer sensitive to the tumbling of the protein. Previous spin labeling studies on annexin B12 have shown that sucrose, aside from slowing the tumbling motion of the protein, does not appear to cause significant structural changes (*11*, *13*). Position 228 had the highest mobility, as evidenced by the high amplitude as well as the sharp and narrowly spaced spectral lines. The high mobility of 228R1 is consistent with its location in the connecting loop between the D and E helices. In contrast, residues that were buried in the X-ray crystal structure (e.g., 237R1) were immobilized on the EPR time scale and gave rise to broad and more distantly spaced EPR spectral lines with well-resolved hyperfine extrema.

Analysis of the EPR spectra for all of the derivatives reveals generally good agreement between the mobility reflected in the EPR spectra and the respective positions in the X-ray crystal structure. To graphically illustrate the correspondence between R1 mobility and local structure, Figure 4A shows the inverse central line width, ΔH_o^{-1}, as a function of sequence number in the nitroxide scan of residues 219−242. ΔH_o^{-1} is frequently used as a semiquantitative measure of R1 mobility, with higher values indicating higher mobility (*24*). Comparison of the experimental ΔH_o^{-1} mobility values to the crystal structure of the protein is further facilitated by considering the fractional solvent accessibility (f_{SA}) of the native residues computed from the crystal structure of annexin B12 (*25*). f_{SA} values for the region of residues 219−242 of annexin B12 are shown in Figure 4B. We will refer to residues with an f_{SA} of ≤ 0.05 as "buried", those with an f_{SA} between 0.05 and 0.25 as "partially solvent accessible", and those with an f_{SA} of >0.25 as "solvent-exposed" (see Figure 4B). Positions with f_{SA} values corresponding to surface sites are marked in blue in both panels A and B of Figure 4, and positions with f_{SA} values corresponding to buried sites are marked in green in both panels. Note that there is reasonably good correspondence between f_{SA} and ΔH_o^{-1}. For example, position 228 has the highest R1 mobility (Figure 4A, black trace) and the highest f_{SA} (Figure 4B). The side chain at position 227 faces the core of the protein (Figure 3) and has low values for both ΔH_o^{-1} (Figure 4A, black trace) and f_{SA} (Figure 4B). The ΔH_o^{-1} values in the region of residues 219−226 exhibited a periodic oscillation that corresponded to the D helix in the crystal structure of the protein. Note local peaks in both ΔH_o^{-1} and f_{SA} values at positions 221 and 225 (Figure 4A,B). The ΔH_o^{-1} values through the E helix region are lower and show less variation than that noted in the D helix. This is consistent with the E helix lacking surface sites and being more buried in the crystal structure than the D helix. Thus, in general, the EPR mobility data throughout this scanned region are in good agreement with the crystal structure of the protein. Together with the functional ability to bind to membranes, these data further demonstrate that the annexin B12 derivatives that were tested still retained a conformation that is highly similar to that of the native protein. Furthermore, the data also reemphasize that the addition of sucrose did not cause significant structural changes.

Oxygen and NiEDDA Accessibility in the Nitroxide Scan of Residues 219−242 of Soluble Annexin B12. The EPR accessibility parameters $\Pi(O_2)$ and Π(NiEDDA) measure the collision rates of these paramagnetic reagents with the R1 side chain. For a soluble protein in aqueous solution, $\Pi(O_2)$ and Π(NiEDDA) are typically in-phase when plotted as a function of residue number (*15*). In addition, both values tend to be closely related to f_{SA} computed from the crystal structure. This expectation is borne out in the data presented in Figure 5A. $\Pi(O_2)$ (black line) and Π(NiEDDA) (red line) are in-phase throughout the nitroxide scan of positions 219−242, and both values show a close correspondence to the computed f_{SA} values (Figure 4B). The color coding of the f_{SA} data in Figure 4B is retained in Figure 5A, and emphasizes the fact that buried residues (green symbols) had low $\Pi(O_2)$ and Π(NiEDDA) values, while surface residues (blue symbols) had high $\Pi(O_2)$ and Π(NiEDDA) values. Both $\Pi(O_2)$ and Π(NiEDDA) values exhibited periodic variation that corresponded to the helical nature of both the D and E helices and, like the mobility parameter ΔH_o^{-1}, were in good agreement with crystallographic data.

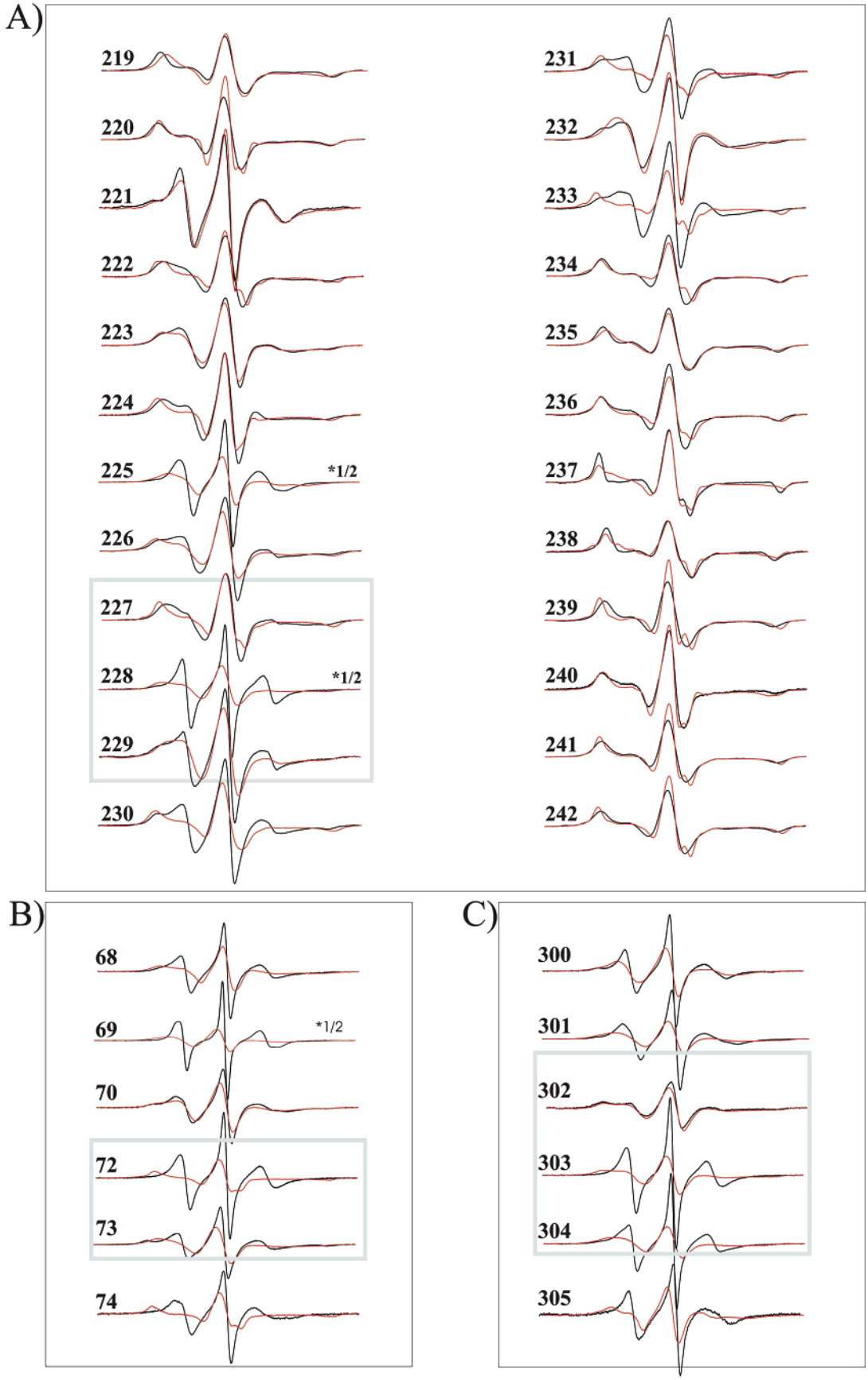

FIGURE 3: EPR spectra of R1-labeled annexin B12. Spectra for annexin B12 containing R1 side chains at the indicated positions were recorded in solution (black traces, 30% sucrose) or following binding to phospholipid vesicles in the presence of Ca^{2+} (red traces; see Experimental Procedures). All spectra were normalized to the same number of spins. The positions of the interhelical loops are denoted with gray boxes; only two spectra are boxed for repeat 1, because 71R1 was unstable and is not shown here. For clarity of presentation, the amplitudes of the indicated spectra recorded in solution were reduced by one-half.

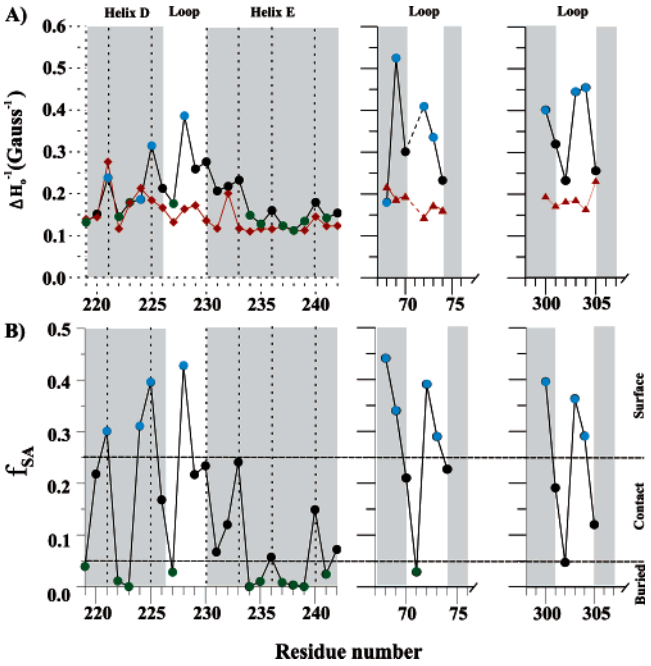

FIGURE 4: Sequence dependence of R1 mobility and fractional solvent accessibility. (A) On the basis of data presented in Figure 3, the inverse of the central line width values (ΔH_o^{-1}) was determined for R1-labeled mutants of annexin B12, and is shown as a function of amino acid sequence for the protein either in solution (black line) or in the Ca^{2+}-dependent membrane-bound form (red line). Locations of the D and E helices are noted with gray-shaded boxes. The individual residues of the protein in solution are color-coded on the basis of fractional solvent accessibility values (see below). The oscillatory nature of the α-helical regions of the protein is highlighted by vertical dashed lines that correspond to peak fractional solvent accessibility values (see below). (B) The fractional solvent accessibility (f_{SA}) of the native residues was computed from the monomer of the crystallographic annexin B12 hexamer (ref *25* and PDB entry 1AEI) and is shown as a function of amino acid sequence. The horizontal dashed lines define the boundaries between buried, partially solvent accessible (contact), and solvent accessible (surface) residues. Individual residues are color-coded on the basis of f_{SA}, with blue indicating surface, green indicating buried, and black indicating contact. The same color scheme is applied to the soluble form of the protein in panel A.

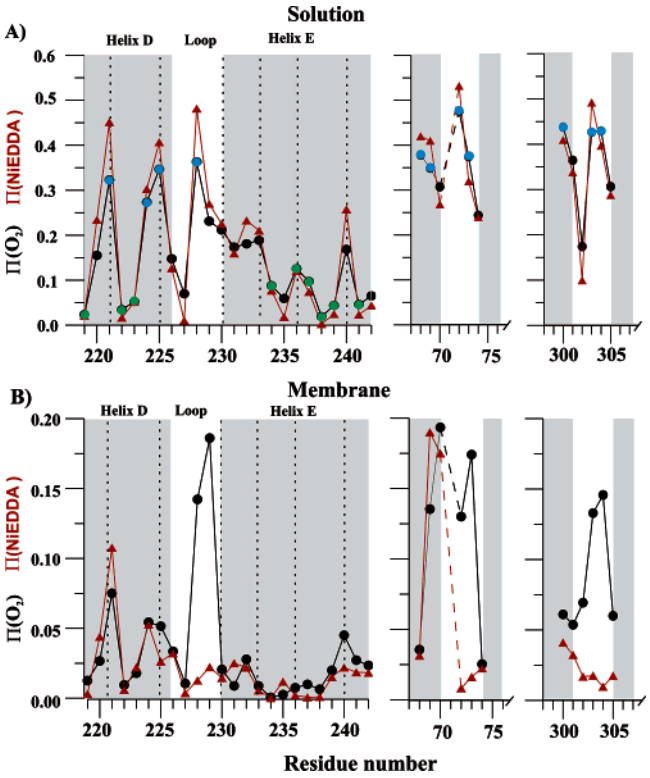

FIGURE 5: Sequence dependence of R1 accessibility in the soluble and membrane-bound states. Accessibility parameters Π(O_2) (black lines) and Π(NiEDDA) (red lines) for R1 side chains are shown as a function of sequence position for R1-labeled annexin B12 derivatives in the soluble state (A) and following Ca^{2+}-dependent binding to membranes (B). Panel A highlights individual residuals with f_{SA} values corresponding to surface sites (blue circles) or buried sites (green circles) as defined in Figure 4B. The oscillatory nature of the α-helical regions of the protein is highlighted by vertical dashed lines that correspond to peak fractional solvent accessibility values (see Figure 4).

Careful inspection of the Π(O_2) and Π(NiEDDA) values showed that several of the deeply buried sites were inaccessible to NiEDDA, but had limited yet measurable accessibility to O_2 (e.g., see 222R1, 227R1, and 235R1 in Figure 5A). Thus, as previously noted in other studies of soluble proteins (*11*, *26*), O_2 appeared to penetrate deeper into the core of this region than the larger and more polar NiEDDA complex.

Membrane-Induced Changes in the Nitroxide Scan of Residues 219−242 of Annexin B12. While Π(O_2) and Π(NiEDDA) values are typically in-phase for soluble proteins, this relationship usually does not apply in regions wherein proteins contact membranes (*15*). Since O_2 preferentially partitions into the hydrophobic core of bilayers and NiEDDA preferentially partitions toward the outside of the bilayer, the Π(O_2)/Π(NiEDDA) ratio is elevated for sites that directly interact with membranes and provides a powerful tool for determining the topography of membrane proteins (*15*). This experimental approach was used to evaluate which regions of annexin B12 come into contact with the bilayer and which regions are exposed to the aqueous environment.

The EPR parameters of the R1 scan of residues 219−242 were recorded after the derivatives were bound to large phospholipid vesicles (2:1 PS:PC ratio) in the presence of Ca^{2+} at pH 7.4. Data presented in Figure 5B show that Π(O_2) and Π(NiEDDA) values were in-phase at most sites in the region of residues 219−242 of the membrane-bound form of annexin B12. The two-turn D helix was readily recognizable by periodic changes in Π(O_2) and Π(NiEDDA). The accessibility of residues in the first two turns of the E helix was reduced relative to values for these sites in the soluble protein, but the Π(O_2) and Π(NiEDDA) values were approximately in-phase. Thus, the overall backbone fold of the protein in these two helical regions appeared to be the same in solution and following Ca^{2+}-dependent binding to membranes. There was no indication that these regions of the protein interacted directly with the bilayer.

In contrast to the helical regions, residues in or near the loop separating the two helices underwent major changes in Π(O_2) and Π(NiEDDA) following membrane binding. Positions 228R1 and 229R1 had very high Π(O_2) and low Π(NiEDDA) values, a clear indication that these R1 side chains were exposed to the hydrophobic region of the bilayer. A plot of Π(O_2)/Π(NiEDDA) for the membrane-bound protein as a function of sequence number is shown in Figure 6 [sites with Π(O_2) and Π(NiEDDA) values near zero were excluded from this analysis for reasons outlined in the legend of Figure 6]. A dramatic peak in Π(O_2)/Π(NiEDDA) was observed at loop residues 228 and 229 (Figure 6). While the Π(O_2)/Π(NiEDDA) values for these residues were ~10

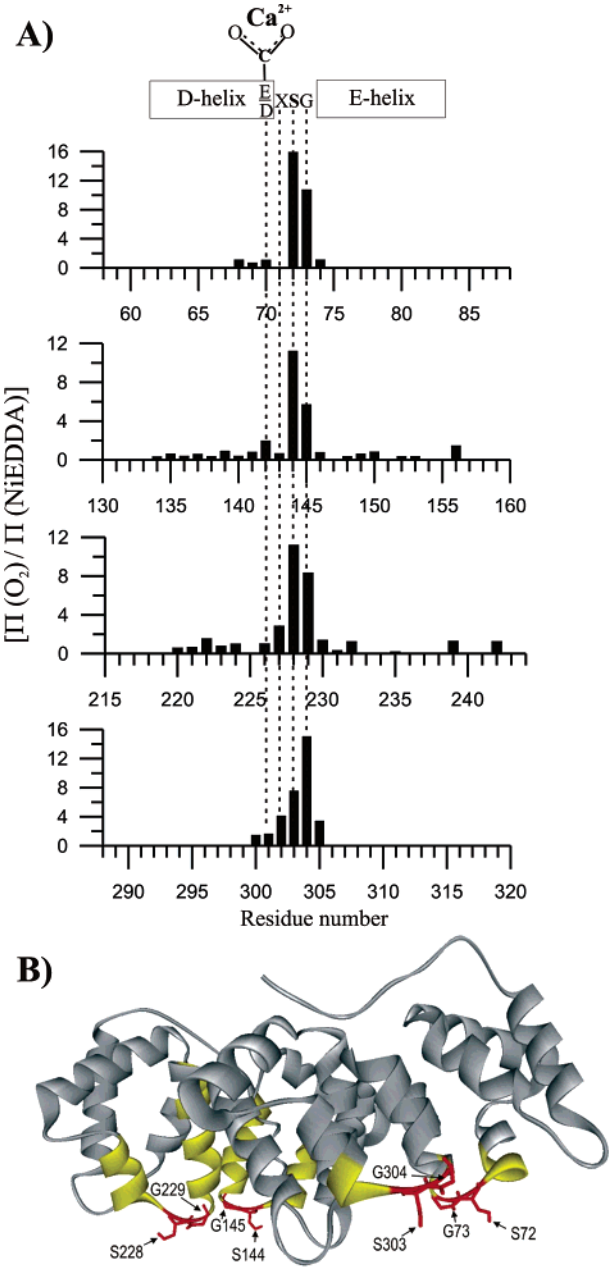

FIGURE 6: Sequence dependence of the ratio of oxygen:NiEDDA accessibility for membrane-bound R1-labeled annexin B12. (A) The values of $\Pi(O_2)$ and Π(NiEDDA) for R1-labeled annexin B12 in the Ca^{2+}-dependent membrane-bound state were taken from Figure 5B for regions in the first, third, and fourth repeats of the protein and from a previous publication (*13*) for the second repeat. The $\Pi(O_2)/\Pi$(NiEDDA) value was plotted as a function of amino acid sequence, with the four repeats of annexin B12 stacked so that homologous positions were aligned vertically. High values for $\Pi(O_2)/\Pi$(NiEDDA) indicate a site that directly associates with the membrane. Sites with $\Pi(O_2)$ and Π(NiEDDA) values near zero were excluded from analysis because dividing small numbers that are dominated by experimental noise produced erratic quotients. On the basis of the low $\Pi(O_2)$ values of these excluded sites, it is clear that they were deeply buried in the core of the protein in both the soluble and membrane-bound forms and clearly were not in contact with the membrane. The model above the plot denotes the positions of the D and E helices and the conserved -D/E-X-S-G- sequence, where the carboxylate group on the D−E residues contributes to formation of the type II Ca^{2+}-binding site. The $\Pi(O_2)/\Pi$(NiEDDA) values for the soluble forms of R1-labeled annexin B12 derivatives were near 1.0 (range of approximately 0.6−1.5), and there were no elevated values in the loop regions (data not shown). (B) Model of the crystal structure of annexin B12 with the sites of the conserved Ser and Gly residues in the D−E loops highlighted.

in the membrane-bound state (Figure 6), the values were ~1 in the soluble state (data not shown). No residues in the region of residues 219−241 had $\Pi(O_2)/\Pi$(NiEDDA) values of >1.5 in the absence of membranes. These results clearly show that the R1 side chain at positions 228 and 229 inserted into the hydrophobic region of the bilayer (see the Discussion).

The other amino acid in the loop between the D and E helices, Phe227, is flanked by Ser228, which inserted into the bilayer, and by Glu226, which coordinated Ca^{2+} that is thought to bridge the protein and bilayer. Despite the fact that it is flanked by residues that interact strongly with the bilayer, 227R1 had relatively low values for both $\Pi(O_2)$ and Π(NiEDDA) in the membrane-bound state (Figure 5B) and, thus, showed no indication of membrane interaction. These data are consistent with the nitroxide side chain of 227R1 projecting toward the core of the protein and away from the membrane (see Figure 1C).

The structure and dynamics of membrane-bound annexin B12 also were investigated by evaluating the motion of R1 side chains in the nitroxide scan of residues 219−242. Note that there was no need to add sucrose to the membrane-bound annexins since the interaction with large vesicles was sufficient to inhibit protein tumbling. The spectra at most positions were very similar in the soluble (Figure 3A, black traces) and membrane-bound forms (Figure 3A, red traces), thereby indicating that there were no major structural changes in response to Ca^{2+}-dependent membrane binding. A reduction in mobility in some of the residues (230, 231, 233, and 237) in the E helix was noted, but was consistent with a general increase in the extent of ordering and a decrease in mobility in the E helix region in response to the constraints of binding to the membrane (Figures 3A and 4A). However, dramatic changes were observed in the mobility of residues in the vicinity of the loop between the D and E helices (Figures 3A and 4A). The most dramatic membrane-induced change in mobility occurred in 228R1. This site had the highest ΔH_o^{-1} value in solution and one of the lowest in the membrane-bound state (Figure 4A). In the absence of membranes, the EPR spectrum of 228R1 was essentially identical in the presence and absence of high concentrations of Ca^{2+} (data not shown). The strong immobilization of 228R1 is close to the rigid limit, and such immobilization is typically only seen at sites that are buried in the core of proteins. A general property of such buried residues, however, is that they are very inaccessible to colliders, including oxygen. This property obviously does not apply to 228R1. As illustrated in Figure 5, not only is the O_2 accessibility of 228R1 more than 1 order of magnitude higher than that of several buried sites (e.g., 222R1, 227R1, and 235R1) but also its accessibility is even higher than that of surface-exposed sites. Thus, it is clear that the cause of the immobilization experienced at position 228 must be very different from that commonly seen at buried protein residues. Similar immobilization, yet high O_2 accessibility, was previously observed in a homologous position in repeat 2 (*13*). As discussed in detail in ref *13*, it had been concluded that the source of the immobilization experienced by the loop residues must arise from interactions with phospholipid headgroups that are immobilized by specific interactions with annexin B12 rather than from specific protein contacts (also see the Discussion).

A less dramatic, yet significant, reduction in the mobility of 225R1 also was noted following membrane binding (Figures 3A and 4A). Inasmuch as position 225R1 did not exhibit a strong increase in $\Pi(O_2)$ upon membrane binding, this side chain does not appear to insert into the bilayer. The reduced level of motion at this site will be discussed below in the context of similar mobility changes that were observed at homologous positions in the three other repeats of annexin B12.

Membrane-Induced Changes in Other D−E Helical Hairpins of Annexin B12. Our previous study (*13*) and the data presented herein serve to demonstrate that the loops between the D and E helices in the second and third repeats of annexin B12 interacted directly with membranes. The other two D−E loop regions of annexin B12 have similar sequences, backbone folds, and f_{SA} values (see Figure 4B) and, therefore, might also be expected to interact with membranes. To provide a comprehensive evaluation of the interaction of all D−E loop regions of annexin B12 with membranes, we performed short nitroxide scans of the D−E loop regions in the first (residues 68−74, excluding residue 71) and fourth (residues 300−305) repeats of the protein (see Figure 1). The EPR parameters of these R1-labeled derivatives were analyzed while the protein was either in solution or bound to phospholipid vesicles in the presence of Ca^{2+} at pH 7.4.

Striking changes in these regions were observed at 72R1 and 303R1, positions that correspond to conserved serine residues in the center of the loop between the D and E helices (Figure 1). These side chains had high $\Pi(O_2)$ and Π-(NiEDDA) values in solution (Figure 5A), as would be expected from their high f_{SA} values (Figure 4B). However, following Ca^{2+}-dependent membrane binding, these sites had very high $\Pi(O_2)$ and low Π(NiEDDA) values, a clear indication that these sites made direct contact with the membrane. A plot of $\Pi(O_2)/\Pi$(NiEDDA) as a function of sequence number emphasized the site of membrane contact (Figure 6). Positions 72R1 and 303R1 were very dynamic in solution, but strongly immobilized following binding to membranes (Figures 3B,C and 4A), a change that was observed at homologous sites in the other two D−E loops. Exposure of 72R1 or 303R1 to Ca^{2+} in the absence of membranes did not induce any change in ΔH_o^{-1} values or spectral line shapes (data not shown). Contact between these side chains and the membrane undoubtedly was responsible for the strong immobilization observed at these sites in the membrane-bound state. However, the interfacial region of liquid crystalline bilayers is mobile on the EPR time scale (*27*, *28*), and strong membrane-induced reduction in the level of motion of R1 side chains on proteins other than annexin B12 has not been observed. Thus, it appears that the headgroup region of phospholipids in bilayers is immobilized as a consequence of Ca^{2+}-dependent annexin B12 binding (see the Discussion).

R1 side chains at positions 73 and 304, sites of highly conserved glycine residues, also showed immobilization (Figures 3B,C and 4A) and increased $\Pi(O_2)/\Pi$(NiEDDA) ratios (Figures 5 and 6) following binding to membranes. Thus, the R1 labels at those sites also appear to interact directly with the bilayer and to be immobilized by the interfacial region of the bilayer. Following membrane binding, 73R1 exhibited changes in mobility and accessibility parameters that were similar to those observed at the homologous sites, 145R1 and 229R1. R1-labeled position 304 exhibited qualitatively similar behavior, but it was more strongly affected by membrane binding in the sense that its $\Pi(O_2)/\Pi$(NiEDDA) ratio was larger than that of the preceding conserved serine site. These differences between position 304 and other homologous sites could be due to either slightly different rotameric states at position 304 or subtle structural differences in this region. It should be noted that residue 304 is located in the E helix that ends as the carboxyl terminus of the protein and might be conformationally less constrained, as has been proposed for annexin A5 (*29*). Regardless of these details, the two highest $\Pi(O_2)/\Pi$-(NiEDDA) ratios for each D−E region were found for the conserved Ser and Gly residues, suggesting that all of the D−E loop regions interact with the membranes in a similar manner overall.

Positions 69 and 300 are located near the end of the D helix. Both have f_{SA} values indicative of surface exposure approximately equivalent to that of the nearby serine sites (72 and 303) in the center of the loops (Figure 4B). Accessibility parameters for these sites in both the soluble and membrane-bound states are consistent with the side chains being on the surface of the proteins (Figure 5A,B), and there is no indication of direct interaction with membranes (Figure 6). However, both 69R1 and 300R1 experienced significant decreases in mobility following binding to membranes (Figures 3B,C and 4A). Interestingly, positions 141 (*13*) and 225 experienced similar immobilization. As previously suggested (*13*), this ordering is likely to arise from the ordering of the D−E loop region, which, in turn, acts to reduce the local dynamics in the more dynamic C-terminal region of helix D.

Residue 302R1, which is also located in the D−E loop, was moderately mobile in both the solution and membrane-bound states (Figures 3C and 4A), presumably because this side chain points toward the core of the protein. For the membrane-bound state, this notion is further supported by the relatively low $\Pi(O_2)/\Pi$(NiEDDA) ratio of this site, which is smaller than the values of all of the conserved Ser and Gly positions but is similar to the value of the homologous position 227. The homologous loop residue, position 71, did not tolerate R1 labeling and was not analyzed.

DISCUSSION

To investigate the molecular mechanism of Ca^{2+}-dependent membrane interaction in annexin B12, the present study employed SDSL and EPR spectroscopy to examine the structure and dynamics of the D−E helical hairpins. Three separate nitroxide scans were generated that covered all of the D−E loop regions and neighboring residues in repeats 1, 3, and 4. Together with a previous study, which focused on only repeat 2, this work provides a comprehensive analysis of all D−E interhelical loop regions of the protein.

This study shows that all D−E loop regions are involved in membrane interaction and experience a membrane-dependent ordering that had not been observed in other proteins studied by SDSL. Despite these pronounced changes in local dynamics, no major conformational changes could be detected upon membrane interaction. Accessibility measurements clearly established that the conserved Ser and Gly positions in all four D−E loops are the primary membrane

interaction sites (Figure 6A), while the preceding loop position (X in the XSG sequence, Figure 6A), as well as residues in the D and E helices, shows little or no evidence of membrane interaction. As shown in Figure 6B, the conserved Ser and Gly residues in all four loop regions are situated in positions that would be conducive to membrane interaction (Figure 6B), while the first loop position (X) projects back into the protein (see Figure 1C). Therefore, at least for all of the regions scanned thus far, the crystal structure appears to represent a valid structural model for the Ca^{2+}-dependent membrane-bound form.

Further attempts to address the overall structure of Ca^{2+}-dependent membrane-bound annexin B12 must take into consideration the shape of the protein in addition to the above-mentioned effects of annexins on bilayer structure and dynamics. All annexin crystal structures are convex on the face that contains the loops that mediate Ca^{2+}-dependent membrane binding. Since the Ca^{2+} ions bound to these loops are not in the same plane, it has been difficult to envision how such a bent surface could interact with the more planar membranes. Since all of the D−E loop regions of annexin B12 come into direct contact with membranes, it is clear that the potential curvature mismatch between the convex annexin B12 surface and the planar bilayers does not specifically prevent the membrane interaction of any of the repeats. However, these data are insufficient in determining the degree to which domain movements might have occurred. It has been suggested that domain movements in annexins would be sufficient to completely flatten the membrane-bound form of these proteins (*21*). In all annexin structures, repeats 1 and 4 form a tightly packed module and repeats 2 and 3 form another. If upon membrane binding these modules are rotated ∼34° around an axis in the plane of the membrane and approximately perpendicular to the two modules, the Ca^{2+} bound to the loops would then be in a single plane. This proposal is attractive and could easily explain the rather similar modes of membrane interaction observed for each of the four D−E loop regions. However, neither cryo-EM nor AFM studies of annexin A5 (*29*, *30*) have provided any direct experimental support for such a reorganization. The inward face of the cleft that is proposed to undergo the "hinge" motion contains the E helix of the third repeat that was part of the extended nitroxide scan in the study presented here. In this study, no dramatic changes in EPR parameters were noted in this region, which might correspond to this region moving closer to the A helix in the opposing module in response to Ca^{2+}-dependent membrane binding. We did note, however, that some of the cleft-facing sites in helix E (230, 233, and 237) of repeat 3 were among the sites that became more immobilized upon membrane interaction. This increased level of immobilization is likely due to the general ordering in the annexin B12 molecule, but additional contacts resulting from domain reorganizations could have further contributed to this immobilization. Although these data could be rationalized in terms of a model that assumes domain organizations, it should be emphasized that it is by no means necessary to invoke major domain movements. The interesting consequence of a model without major domain reorganizations would be that, unlike the D−E loop sites, the homologous A−B loop regions would lie at a very different immersion depth. While the A−B loop regions in repeats 2 and 4 are located toward the center of the curved surface, the analogous loop regions in repeats 1 and 3 are located toward the periphery. Thus, in the absence of pronounced domain reorganizations, the latter regions might not insert as deeply as the former. Studies are underway to test those structural models.

R1 side chains on all four D−E loops of annexin B12 were strongly immobilized following Ca^{2+}-dependent binding to membranes (Figure 3 and ref *13*). Previous studies failed to detect protein−protein interactions under these conditions (*9*), and accessibility studies clearly established that the loops inserted into bilayers (Figures 5 and 6 and ref *13*). From our previous study of the D−E loop in the second repeat of annexin B12, we concluded that the strong immobilization of loop side chains was due to interaction with the headgroups of the phospholipid bilayer, and the mechanism was discussed in detail (*13*). Our current studies show that similar immobilization occurred in all other D−E loops, and the high O_2 accessibilities of the membrane-exposed residues strongly argue against these residues being immobilized by tight packing interactions with the protein. Collectively, these data further strengthen the conclusion that immobilization of loop side chains was via protein−phospholipid headgroup interaction rather than incidental protein contacts.

Normally, in the absence of annexins, the bilayer has a rather dynamic structure in which phospholipids exhibit a wide range of conformational, rotational, and translational molecular motions that occur over a broad time scale. Time-averaged probability distribution functions of the various chemical groups in phospholipids projected onto the bilayer normally show that a bilayer is composed of a hydrocarbon core flanked by interfacial regions that are defined by significant water accessibility (*31*). These interfacial regions constitute approximately half of the thicknesses of bilayers, and provide a broad and chemically heterogeneous region that interacts with peripheral membrane proteins. The interfacial region occupied by the phospholipid headgroups is the least mobile part of the bilayer, but still is too dynamic to constrain the R1 side chain in the interhelical loops of annexin B12 to the extent observed (see the Discussion in ref *13*). Thus, the ternary phospholipid−Ca^{2+}−annexin complex must induce changes in the bilayer that are sufficient to immobilize the R1 side chains on the EPR time scale. This idea is supported by previous EPR studies of nitroxide-labeled lipids showing that annexin A5 immobilized sites in the vicinity of the phospholipid headgroups, but had minimal effects on sites near the center of the hydrocarbon core of bilayers (*20*). Furthermore, other studies showed that the lateral diffusion of phospholipids (*18*, *32*) and a membrane protein (*33*) was dramatically inhibited by annexins A4, A5, and B12.

Annexins are proposed to serve as biological molecular fences that create or maintain domains of a nonhomogeneous distribution of lipids and/or proteins in cellular membranes (*2*). Our studies showing the immobilized nature of the Ca^{2+}-dependent complex of bilayers and the D−E hairpins in annexin B12 are consistent with this proposal and offer insights into the mechanism by which the bilayers are immobilized. The crucial sequence in the D−E loops of annexin B12, Glu/Asp-X-Ser-Gly, is highly conserved in other annexin gene products found in the animal kingdom (*34*); thus, these annexins may share similar Ca^{2+}-dependent membrane binding properties with annexin B12. However,

the highly conserved serine at the center of these D−E loops is replaced by Lys in two of the four repeats of annexins A1 and A2, two annexins that appear to form a subgroup with membrane binding properties that are distinctively different from those of trimer-forming annexins such as annexins A5 and B12 (*14*). Annexins A1 and A2 have not been reported to strongly immobilize lipids, and our preliminary studies of a D−E helical hairpin in annexin A2 show that it was not as strongly immobilized as the corresponding region in annexin B12 (P. Wu, J. M. Isas, H. T. Haigler, and R. Langen, unpublished results). Thus, annexins A1 and A2 may have biological functions that differ from those of trimer-forming annexins.

REFERENCES

1. Cho, W., and Stahelin, R. V. (2005) Membrane-protein interactions in cell signaling and membrane trafficking, *Annu. Rev. Biophys. Biomol. Struct. 34*, 119−51.
2. Gerke, V., Creutz, C. E., and Moss, S. E. (2005) Annexins: Linking Ca^{2+} signalling to membrane dynamics, *Nat. Rev. Mol. Cell Biol. 6*, 449−61.
3. Rescher, U., and Gerke, V. (2004) Annexins: Unique membrane binding proteins with diverse functions, *J. Cell Sci. 117*, 2631−9.
4. Seaton, B. A. (1996) in *Annexins: Molecular Structure to Cellular Function* (Seaton, B. A., Ed.) R. G. Landes Co., Austin, TX.
5. Moss, S. E., and Morgan, R. O. (2004) The Annexins, *Genome Biol. 5*, 219.
6. Swairjo, M. A., Concha, N. O., Kaetzel, M. A., Dedman, J. R., and Seaton, B. A. (1995) Ca^{2+}-bridging mechanism and phospholipid head group recognition in the membrane-binding protein annexin V, *Nat. Struct. Biol. 2*, 968−74.
7. Huber, R., Schneider, M., Mayr, I., Romisch, J., and Paques, E. P. (1990) The calcium binding sites in human annexin V by crystal structure analysis at 2.0 Å resolution. Implications for membrane binding and calcium channel activity, *FEBS Lett. 275*, 15−21.
8. Gerke, V., and Moss, S. E. (2002) Annexins: From structure to function, *Physiol. Rev. 82*, 331−71.
9. Langen, R., Isas, J. M., Luecke, H., Haigler, T. H., and Hubbell, W. L. (1998) Membrane-mediated assembly of annexins studied by site-directed spin labeling, *J. Biol. Chem. 273*, 22453−7.
10. Langen, R., Isas, J., Hubbell, W., and Haigler, H. (1998) A transmembrane form of annexin XII detected by site-directed spin labeling, *Proc. Natl. Acad. Sci. U.S.A. 95*, 14060−5.
11. Isas, J. M., Langen, R., Haigler, H. T., and Hubbell, W. L. (2002) Structure and dynamics of a helical hairpin and loop region in annexin 12: A site-directed spin labeling study, *Biochemistry 41*, 1464−73.
12. Isas, J. M., Patel, D. R., Jao, C., Jayasinghe, S., Cartailler, J. P., Haigler, H. T., and Langen, R. (2003) Global structural changes in annexin 12. The roles of phospholipid, Ca^{2+}, and pH, *J. Biol. Chem. 278*, 30227−34.
13. Isas, J. M., Langen, R., Hubbell, W. L., and Haigler, H. T. (2004) Structure and dynamics of a helical hairpin that mediates calcium-dependent membrane binding of annexin B12, *J. Biol. Chem. 279*, 32492−8.
14. Patel, D., Isas, J., Ladokhin, A., Jao, C., Kim, Y., Kirsch, T., Langen, R., and Haigler, H. (2005) The Conserved Core Domains of Annexins A1, A2, A5 and B12 Can Be Divided into Two Groups with Different Calcium-Dependent Membrane-Binding Properties, *Biochemistry 44*, 2833−44.
15. Hubbell, W. L., Gross, A., Langen, R., and Lietzow, M. A. (1998) Recent advances in site-directed spin labeling of proteins, *Curr. Opin. Struct. Biol. 8*, 649−56.
16. Columbus, L., and Hubbell, W. L. (2002) A new spin on protein dynamics, *Trends Biochem. Sci. 27*, 288−95.
17. Altenbach, C., Greenhalgh, D. A., Khorana, H. G., and Hubbell, W. L. (1994) A collision gradient method to determine the immersion depth of nitroxides in lipid bilayers: Application to spin-labeled mutants of bacteriorhodopsin, *Proc. Natl. Acad. Sci. U.S.A. 91*, 2910.
18. Gilmanshin, R., Creutz, C. E., and Tamm, L. K. (1994) Annexin IV reduces the rate of lateral lipid diffusion and changes the fluid phase structure of the lipid bilayer when it binds to negatively charged membranes in the presence of calcium, *Biochemistry 33*, 8225−32.
19. Saurel, O., Cézanne, L., Milon, A., Tocanne, J., and Demange, P. (1998) Influence of annexin V on the structure and dynamics of phosphatidylcholine/phosphatidylserine bilayers: A fluorescence and NMR study, *Biochemistry 37*, 1403−10.
20. Megli, F. M., Selvaggi, M., Liemann, S., Quagliariello, E., and Huber, R. (1998) The calcium-dependent binding of annexin V to phospholipid vesicles influences the bilayer inner fluidity gradient, *Biochemistry 37*, 10540−6.
21. Voges, D. B., Burger, A., Demange, P., Baumeister, W., and Huber, R. (1994) Three-dimensional structure of membrane-bound annexin V. A correlative electron microscopy−X-ray crystallography study, *J. Mol. Biol. 238*, 199−213.
22. Reeves, J. P., and Dowben, R. M. (1969) Formation and properties of thin-walled phospholipid vesicles, *J. Cell. Physiol. 73*, 49−60.
23. Koradi, R., Billeter, M., and Wuthrich, K. (1996) MOLMOL: A program for display and analysis of macromolecular structures, *J. Mol. Graphics 14*, 51−5, 29−32.
24. McHaourab, H. S., Lietzow, M. A., Hideg, K., and Hubbell, W. L. (1996) Motion of spin-labeled side chains in T4 lysozyme. Correlation with protein structure and dynamics, *J. Biol. Chem. 273*, 810−2.
25. Luecke, H., Chang, B. T., Mailliard, W. S., Schlaepfer, D. D., and Haigler, H. T. (1995) Crystal structure of the annexin XII hexamer and implications for bilayer insertion, *Nature 378*, 512−5.
26. Oh, K. J., Zhan, H., Cui, C., Altenbach, C., Hubbell, W. L., and Collier, R. J. (1999) Conformation of the diphtheria toxin T domain in membranes: A site-directed spin-labeling study of the TH8 helix and TL5 loop, *Biochemistry 38*, 10336−43.
27. Devaux, P., and McConnell, H. M. (1972) Lateral diffusion in spin-labeled phosphatidylcholine multilayers, *J. Am. Chem. Soc. 94*, 4475−81.
28. Hubbell, W. L., and McConnell, H. M. (1971) Molecular motion in spin-labeled phospholipids and membranes, *J. Am. Chem. Soc. 93*, 314−26.
29. Oling, F., Santos, J. S., Govorukhina, N., Mazeres-Dubut, C., Bergsma-Schutter, W., Oostergetel, G., Keegstra, W., Lambert, O., Lewit-Bentley, A., and Brisson, A. (2000) Structure of membrane-bound annexin A5 trimers: A hybrid cryo-EM−X-ray crystallography study, *J. Mol. Biol. 304*, 561−73.
30. Reviakine, I., Bergsma-Schutter, W., Mazeres-Dubut, C., Govorukhina, N., and Brisson, A. (2000) Surface topography of the p3 and p6 annexin V crystal forms determined by atomic force microscopy, *J. Struct. Biol. 131*, 234−9.
31. White, S. H., Ladokhin, A. S., Jayasinghe, S., and Hristova, K. (2001) How membranes shape protein structure, *J. Biol. Chem. 276*, 32395−8.
32. Saurel, O., Cezanne, L., Milon, A., Tocanne, J. F., and Demange, P. (1998) Influence of annexin V on the structure and dynamics of phosphatidylcholine/phosphatidylserine bilayers: A fluorescence and NMR study, *Biochemistry 37*, 1403−10.
33. Peng, S., Publicover, N. G., Airey, J. A., Hall, J. E., Haigler, H. T., Jiang, D., Chen, S. R., and Sutko, J. L. (2004) Diffusion of single cardiac ryanodine receptors in lipid bilayers is decreased by annexin 12, *Biophys. J. 86*, 145−51.
34. Morgan, R. O., and Fernández, M. P. (1997) Annexin gene structures and molecular evolutionary genetics, *Cell. Mol. Life Sci. 53*, 508−15.

BI051751M